



### Science Arts & Métiers (SAM)

is an open access repository that collects the work of Arts et Métiers Institute of Technology researchers and makes it freely available over the web where possible.

This is an author-deposited version published in: <https://sam.ensam.eu>  
Handle ID: <http://hdl.handle.net/10985/23049>



This document is available under CC BY license

#### To cite this version :

Jinlin GONG, Benteng ZHAO, Youxi HUANG, Eric SEMAIL, Ngac Ky NGUYEN - Quantitative Comparisons of Outer-Rotor Permanent Magnet Machines of Different Structures/Phases for In-Wheel Electrical Vehicle Application - Energies - Vol. 15, n°18, p.6688 - 2022




Any correspondence concerning this service should be sent to the repository

Administrator : [archiveouverte@ensam.eu](mailto:archiveouverte@ensam.eu)



## Article

# Quantitative Comparisons of Outer-Rotor Permanent Magnet Machines of Different Structures/Phases for In-Wheel Electrical Vehicle Application

Jinlin Gong <sup>1,\*</sup>, Benteng Zhao <sup>1,2</sup>, Youxi Huang <sup>1</sup>, Eric Semail <sup>3</sup> and Ngac Ky Nguyen <sup>3</sup><sup>1</sup> School of Electrical Engineering, Shandong University, Jinan 250061, China<sup>2</sup> China Astronaut Research and Training Center, Beijing 100094, China<sup>3</sup> Laboratory of Electrical Engineering and Power Electronics of Lille (L2ep), Arts et Métiers, 59043 Lille, France

\* Correspondence: gongjinlin@sdu.edu.cn

**Abstract:** As one of the key components, low-speed direct-drive in-wheel machines with high compact volume and high torque density are important for the traction system of electric vehicles (EVs). This paper introduces four different types of outer-rotor permanent magnet motors for EVs, including one five-phase SPM machine, one three-phase IPM machine with V-shaped PMs, one seven-phase axial flux machine (AFM) of sandwich structure and finally one hybrid flux (radial and axial) machine with a third rotor with V-shaped PMs added to the AFM. Firstly, the design criteria and basic operation principle are compared and discussed. Then, the key properties are analyzed using the Finite Element Method (FEM). The electromagnetic properties of the four fractional slot tooth concentrated winding in-wheel motors with similar dimensions are quantitatively compared, including air-gap flux density, electromotive force, field weakening capability, torque density, losses, and fault tolerant capability. The results show that the multi-phase motors have high torque density and high fault tolerance and are suitable for direct drive applications in EVs.

**Keywords:** permanent magnet machine; SPM machine; IPM machine; axial flux machine; hybrid flux machine; multiphase machine; outer-rotor; electric vehicle



**Citation:** Gong, J.; Zhao, B.; Huang, Y.; Semail, E.; Nguyen, N.K.

Quantitative Comparisons of Outer-Rotor Permanent Magnet Machines of Different Structures/Phases for In-Wheel Electrical Vehicle Application. *Energies* **2022**, *15*, 6688. <https://doi.org/10.3390/en15186688>

Academic Editor: Adolfo Danniier

Received: 20 July 2022

Accepted: 7 September 2022

Published: 13 September 2022

**Publisher's Note:** MDPI stays neutral with regard to jurisdictional claims in published maps and institutional affiliations.



**Copyright:** © 2022 by the authors. Licensee MDPI, Basel, Switzerland. This article is an open access article distributed under the terms and conditions of the Creative Commons Attribution (CC BY) license (<https://creativecommons.org/licenses/by/4.0/>).

## 1. Introduction

Electric vehicles (EVs) have been developed with great effort in recent years, due to both energy and environment issues [1]. Compared to traditional internal combustion engine (ICE) vehicles, EVs are friendlier to the environment, e.g., less noisy and less air pollution, which also makes them more comfortable to the passengers.

As one of the key components, electrical machines with high performances are important for the traction system of EVs. Some specifications should be therefore satisfied, such as high torque density and high functional reliability [2]. Several successful designs and applications of the direct- and indirect-driven motors and drives on the EVs have been proposed. Two typical kinds of applications are commercialized: the first one is a high-speed machine together with transmission gear, which are characterized by high power density [3], and the second one is a low-speed direct-drive motor, which is characterized by high torque density [4]. Due to the high integration level and high torque density, EVs driven by in-wheel machines are considered as a good choice for future transportation [5]. For in-wheel traction application, the aim of low speed, high torque, and high reliability are the key requirements [6]. In the following part of the introduction, different methods to achieve the high torque density are summarized. Firstly, the methods for improvement of torque density are generally concluded, and then, the different high torque density structures of PM machines for in-wheel driven applications are covered. Finally, the effects of the phase numbers on the performance of reliability are analyzed.

In [4], the methods to improve the torque density are summarized. The first one is the use of cobalt iron (CoFe) lamination instead of silicon steel lamination; the maximum electromagnetic load can be increased by using this material. The superiority in terms of volume, mass and torque density are achieved by using CoFe lamination. Tooth concentrated winding technology together with open slots make it easier to manufacture with a higher slot fill factor and thus a higher torque density. The reluctance torque is reinforced in PM machines in order to improve the torque density in the low speed region and extend the speed range in the high speed region [5]. The interior PM machines are thus more preferred than the surface-mounted PM (SPM) machines due to the use of the reluctance torque. The torque density of machines can also be improved by changing the machine structure. In the following part, different types of machines used for in-wheel application are compared, i.e., radial flux machines and axial flux machines.

Many kinds of machines can be used in wheel machines. They can be categorized by the flux direction as radial flux machine, axial flux machine, and transversal flux machine. In [7], a new self-decelerating PM in-wheel motor for low-speed and high-torque drive was proposed using magnetic gear. The proposed machine has two air gaps. In [8], by optimizing the shape of PMs, the outer rotor flux switching PM machine exhibits better flux-weakening capability and high efficiency and wider speed range. In [9], V-shaped magnets embedded in the external rotor to achieve enhanced magnetic flux concentration and hence high torque density was designed for low-speed E-bike application. In [10], a modular spoke type permanent-magnet machine for in-wheel applications was proposed and compared to three-phase SPM machines and a commercial machine; both torque capability and flux weakening capability were improved. In [11], two wheel-motors for light passenger cars were compared: axial and radial flux machine. Under the constraint of the same volume, the same speed and the flux density in the air gap, the axial flux machine had better torque density both in terms of volume and mass. The AFM is preferred in low-speed applications and with constrained axial length. In [12], a double stator and single rotor axial flux motor was optimally designed. In [13], based on a radial flux modulation machine, an axial flux modulation machine was designed and compared. For in-wheel drive of HEVs, the AFM has higher power density and a simpler manufacture process, but the axial forces can be at the origin of mechanical problems.

The field modulation effect/magnetic gearing effect is also one of the ways to improve torque density, and the field-modulated permanent-magnet machines such as permanent magnet vernier machines (PMVMs) are also suitable for low-speed and high-torque applications. High amplitudes and a large variation gradient of armature working harmonic that have the same pole-pair of PMs lead to the high-torque density of PMVMs [14]. In [15], a fault-tolerant PMVM was designed for direct-drive applications, which has merits of high-torque density and high reliability.

#### *The Effects of the Number of Phase*

##### (a) Torque density improvement with optimal third harmonic (supply or PM shape)

For three-phase PM machines in star connection, the fundamental air gap flux density of PMs can be improved by a PM-shaping technique with optimal third harmonics in the radial direction, and the torque density can be improved by 9% [16]. Along the axial direction, a novel machine of a shaped magnet with an optimal third harmonic is proposed in [17]. Fifteen percent higher torque with zero pulsation can be achieved. The above illustrations about the in-wheel motors all focus on the three-phase machines. Another alternative to improve the torque density and the extend operational speed range is multiphase machines. Due to the development of power electronics and a semi-silicon conductor, multiphase machines have been developed quickly in recent decades. Compared to three-phase machines, the output torque can be improved through the injection of higher-order harmonic currents related to no-sinusoidal back-emf of PM machines. By considering the third harmonic both on the PM shape and the current supply, the torque density can be increased by 30%, compared to a five-phase sinusoidal machine, with the same level of

torque pulsation [18]. In [19], a novel bi-harmonic five-phase machine was proposed, which could develop torque of comparable values under three kinds of supply: with only first, third or both first and third sinusoidal current. Both the torque density at low speed and the operation range at high speed were improved. Therefore, with PM multiphase machines of a high number of phases, it is then possible to obtain the same high-torque density of three-phase DC brushless machines, with trapezoidal emf and currents, but without torque pulsation. Compared to non-sinusoidal machines, e.g., brushless dc machines, the output torque can be improved with high quality and less torque pulsation.

#### (b) Fault-tolerant capability

Multiphase machines can be found in the critical application requiring high fault-tolerant capability [20], for example, sub-marine propulsion, aerospace and certainly EVs. For three-phase machines without a neutral point connection, the loss of one phase fails to generate a rotating magnetic field with a breakdown for the machines. Therefore, three is effectively the minimum number of phases allowed to generate the required rotating field for a machine. In the case of multiphase machines, even if one phase is open-circuited, it can still work without stopping. The current in health mode should be rearranged in order to reduce the torque pulsation [21,22] for sinusoidal machines. The constraints on current and voltage limit per phase are considered in faulty modes for a non-sinusoidal seven-phase machine [23]. By imposing current in the main and secondary machines, the machine can output 56% of healthy torque without pulsation. Using reduce order matrix transformation, the constant current in the d-q frame can be obtained, which makes it easier to control with a PI controller [24]. For non-sinusoidal machines, the transformation matrix related to the third harmonic current is proposed, and the third harmonic current is optimally injected without a torque ripple [25].

In this paper, a quantitative comparison of the outer-rotor in-wheel motors of different structures and phases is presented. A commercial five-phase SPM machine is taken as reference [26], and a three-phase V-shaped IPM machine [9] and a seven-phase axial flux machine (AFM) are designed. Based on the previous AFM machine, a third rotor with V-shaped PMs of different poles is designed [27], which is a hybrid flux (radial and axial) machine (HFM). Considering the magnetic flux direction, PM shape and the number of phases, four machines were selected for comparison. The magnetic flux direction includes radial magnetic flux, axial magnetic flux, and hybrid magnetic flux. PM shape includes built-in V shape and surface mounted. The number of phases are three, five, and seven. The original intention of the seven-phase HFM design is to use the winding ends to increase the output torque of the motor. In addition, the third rotor can replace the “radial frame” for the “motor enclosure”, which gives the seven-phase HFM an advantage when compared to an enclosed motor. The aim is to show the differences of the four machines in terms of structure and the advantage of increasing the of number of phases. The paper is organized as follows. The design criteria and basic operating principle are described in Section 2. A quantitative comparison in healthy mode operation is given in Section 3, including air gap flux density, emf, flux weakening capability and torque density. Then the fault-tolerant capabilities are compared in Section 4. Finally, the conclusion of the comparison is given in Section 5.

## 2. Design and Operational Principle of Four In-Wheel Motors

Non-overlapping, all or alternate teeth wound windings will be referred to as fractional slot concentrated winding (FSCW) for the rest of this paper [28], which has a fractional slot per pole and per phase. All four machines are with FSCW, which is a good candidate for wheel-hub propulsion due to short-end winding, high-torque density and superior flux weakening ability [29]. In order to maximize the output torque, the choice of slot/pole

combination of FSCW with a high winding factor is often priority. Using winding function theory [30], the winding factors of any winding can be deduced:

$$K_h = \frac{N}{N_s} \left| \sum_{m=0}^{N_s-1} d_{m,n} e^{-j \frac{2\pi}{N_s} m p h} \right| \quad (1)$$

where  $N$  and  $N_s$  are the number of phases and slots, respectively;  $d_{m,n}$  is the element of distribution matrix;  $p$  is the pole-pair number;  $h$  is the harmonic order. The fundamental winding factor ( $h = 1$ ) is concerned for three-phase machines, and the higher orders of the winding factor are also concerned for multiphase ( $>3$ ) machines, especially for non-sinusoidal multiphase machines.

One of the key challenges of FSCW is the additional stator magnetomotive force (MMF) sub-and super-harmonics that leads to higher losses as well as saturation effects [31]. MMF of any winding can be deduced as follows [30]:

$$mmf(\theta_s, t) = \sum_{n=0}^{N-1} N_n(\theta_s) i_n(t) \quad (2)$$

where  $N_n(\theta_s)$  is the winding function related to the distribution of conductor in the slots, and  $\theta_s$  is the angle respected to the stator;  $i_n(t)$  is the injected current. Thus, the MMF distribution varies with respect to both time and space.

In order to quantitatively evaluate the content of non-working harmonics of MMF, THD is defined as follows:

$$THD = \sqrt{\sum_{n \neq w}^H \left( \frac{mmf_n}{mmf_w} \right)^2} \quad (3)$$

where  $H$  is the number of harmonics to be considered;  $w$  is the order of working harmonics.

The design details of the four proposed machines are presented in this part. Figure 1 shows the basic configurations, in which Figure 1a relates to the five-phase SPM machine, which is commercialized for E-bikes; Figure 1b is a three-phase IPM machine with V-shaped PMs, and the original idea, e.g., a combination of slot/pole, is presented in [9]. Figure 1c shows the seven-phase AFM machine of a sandwich structure, i.e., double outer-rotors and one stator. A third rotor with V-shapes PMs is added to the AFM, and a hybrid flux (radial and axial) machine is constructed, as shown in Figure 1d. The initial idea of this hybrid flux machine is to take advantage of the end winding and to reinforce the output torque.

In Figure 1, the stator windings are color-coded as follows. The phase A, B, C, D and E windings of the five-phase SPM machine are represented by deep red, yellow, green, blue and pink, respectively; the phase A, B and C windings of the three-phase IPM machine are respectively represented by red, yellow and blue; the phase A, B, C, D, E, F and G windings of the seven-phase AFM or HFM machine are represented by deep red, pink, yellow, blue, brown, bottle-green and silver, respectively. The scale bars are added for easy size comparison. Please note, the four machines do not share the same scale bars.

In order to achieve a fair comparison between these four machines, based on the commercial five-phase SPM machine, the following considerations are taken into account:

- For the three-phase IPM machine, the outer rotor and stator radius, the air gap, and the copper and iron are the same for the five-phase machine;
- For the seven-phase HFM machine, the air gap, the outer radius and the axial length of the third rotor are the same in reference to the five-phase machine. Thus, the global volume of these two machines is the same;
- For the seven-phase AFM machine, the difference with the seven-phase HFM is that it has not a radial rotor;
- All four machines have the same amplitude of air gap flux density and the same slot filling factor;

- The injected phase current density is kept the same, and the nominal phase voltage is the same for all machines.

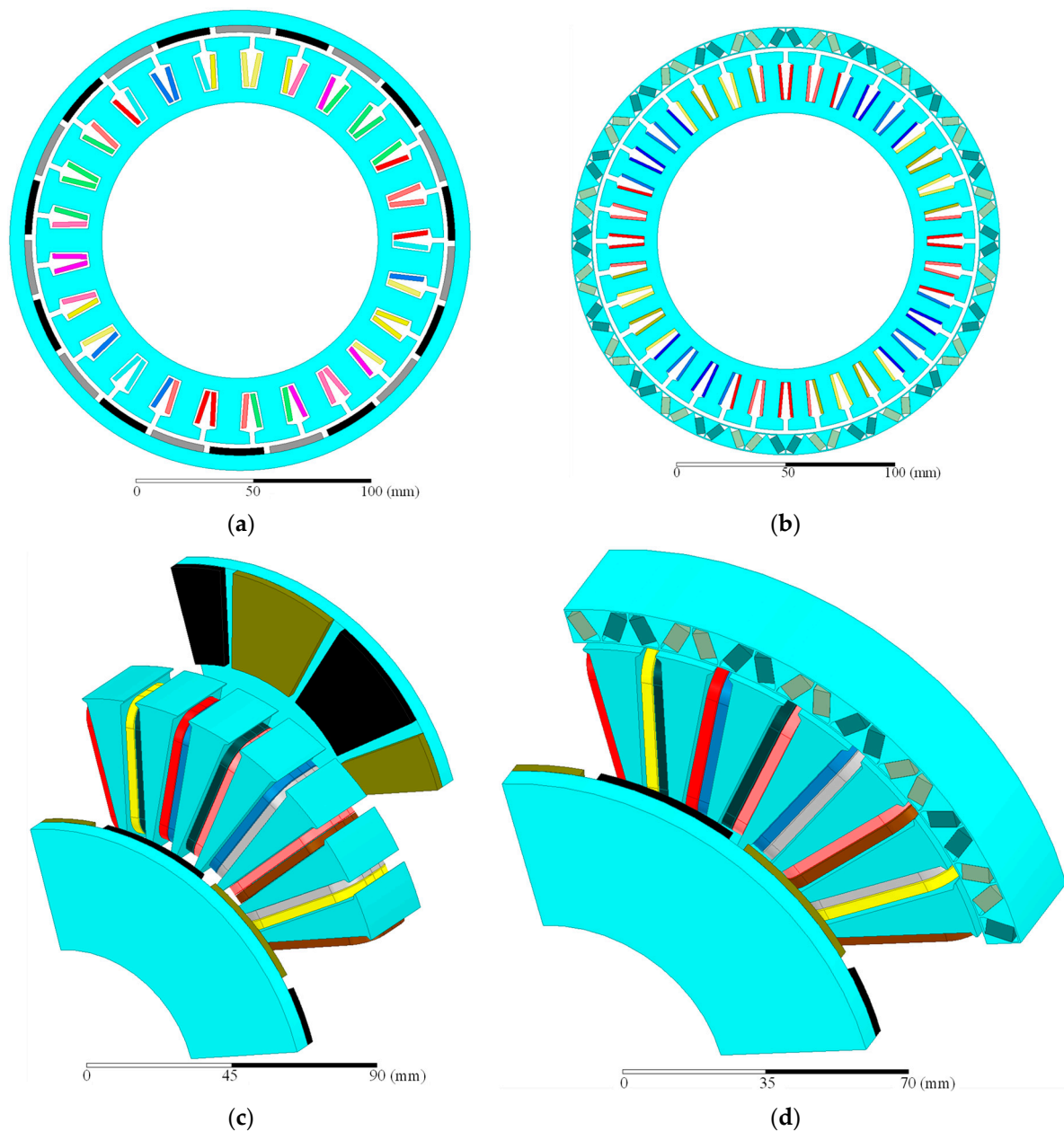


**Figure 1.** Four types of outer-rotor in-wheel motors: (a) five-phase SPM; (b) three-phase V-shaped IPM; (c) seven-phase AFM; (d) seven-phase HFM.

### 2.1. Five-Phase SPM

The five-phase SPM machine is a commercial one for E-bikes, as shown in Figure 1a. The PMs are surface-mounted onto the rotor, which makes it easier for production. In order to increase the output torque, the in-wheel machines often have a big value of radius of the outer-rotor, and thus, there is much space in the inner stator. Therefore, the in-wheel outer-rotor machines have good performance of torque density in terms of mass and not volume.

A double-layer FSCW is adopted, and it consists of 25 slots and 22 poles. There is a fundamental winding factor  $K_1$  that is 0.97, and the third harmonic winding factor  $K_3$  is 0.73. The MMF distribution is calculated according to the injection of a fundamental

and the third harmonic current. Figure 2 shows the MMF harmonics spectrum, with the injection of the fundamental and the third harmonic current. It can be noted that with the fundamental current injection, the 11th harmonic is of maximum amplitude, which consists of the number of pole-pairs. However, there is a super-harmonic (14th) that is also of big value of amplitude, it is thus not suitable for high-speed application since it is at the origin of eddy currents. Under the injection of the third harmonic current, the amplitude of the working harmonic ( $h = 33$ ) is much smaller compared to other sub- and super-harmonics. It is thus not interesting to inject the third harmonic current for this machine. The THD of MMF with fundamental current harmonic injection is 0.923 according to (3). All the above analysis demonstrate that it is suitable for low-speed applications.

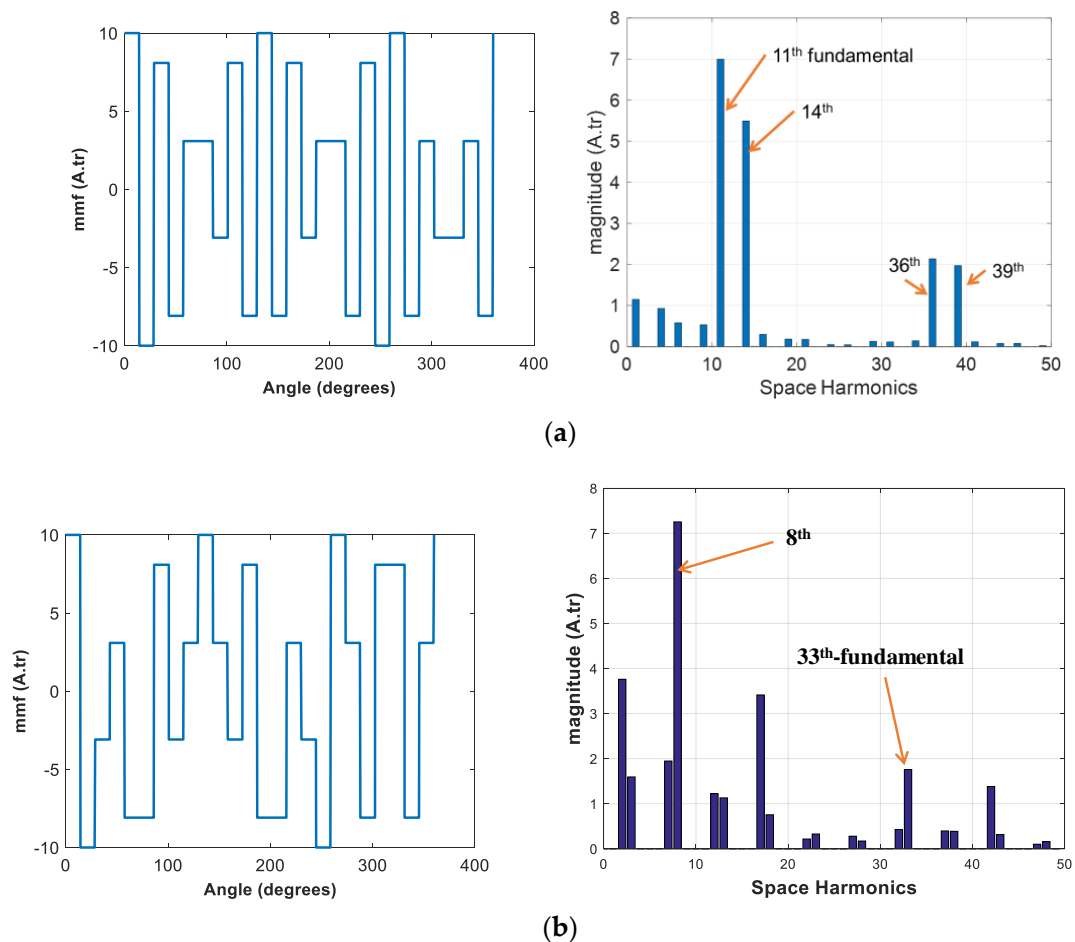


**Figure 2.** MMF harmonic spectrum of five-phase SPM with fundamental current and third harmonic current: (a) fundamental harmonic; (b) third harmonic.

## 2.2. Three-Phase IPM

The three-phase IPM machine is also designed for E-bike application. The V-shaped magnets are embedded in the outer-rotor to achieve enhanced magnetic flux concentration and hence high power and high torque output [9]. Compared to SPM machines, IPM machines have higher torque density due to the difference between the d- and q-axis inductance, which can contribute to the reluctance. Moreover, the PMs are embedded on the rotor, which makes it easier to assemble and produce.

The IPM machine consists of 36 slots and 32 poles, which are selected according to the higher value of the greatest common divisor (GCD) in order to have a smaller cogging torque. The fundamental winding factor  $K_1$  is 0.945. For a three-phase machine in star connection, the third harmonic current cannot be used to improve the output torque; thus, the third harmonic winding factor is not concerned. The MMF distribution and its spectrum

are shown in Figure 3. The working harmonic is the 16th, considered as the fundamental one, and the 20th, with a big value of amplitude, is a parasitic sup-harmonic that is the main harmonic leading to iron losses and eddy current losses of PMs. The THD of MMF is 0.897 according to (3). All the above analysis demonstrate that it is suitable for low speed applications.

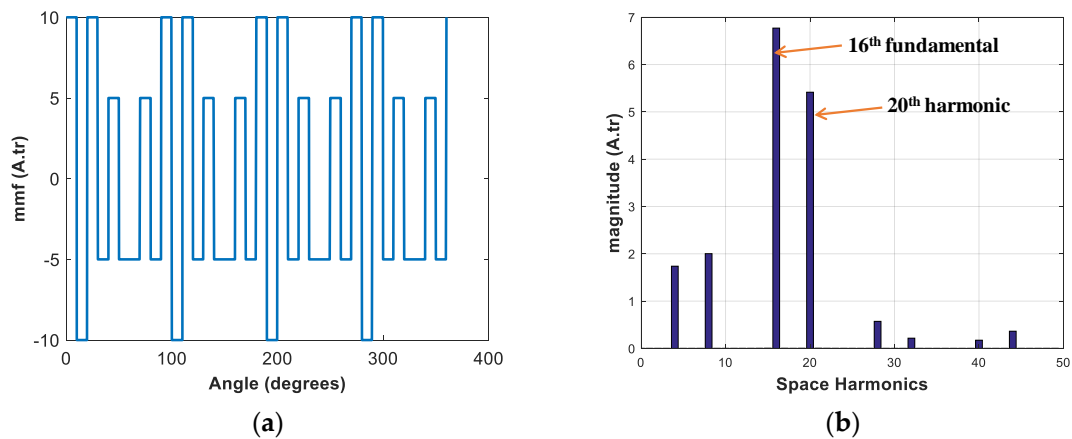


**Figure 3.** MMF harmonic spectrum of three-phase IPM with fundamental current: (a) MMF; (b) harmonic spectrum.

### 2.3. Seven-Phase AFM

The seven-phase machine is an axial flux machine, as shown in Figure 1c. It is a sandwich structure, i.e., two outer-rotors with PMs surface mounted and one stator with tooth concentrated winding. It consists of 28 slots and 12 poles. The initial winding factors for this combination are  $K_1 = 0.623$  and  $K_3 = 0.901$ . The winding is therefore rearranged using the stator shifting method, and the winding factors for the new winding are  $K_1 = 0.975$  and  $K_3 = 0.782$ .

The MMF distribution with the fundamental and third harmonic current injection is shown in Figure 4. Under the fundamental current injection, the working harmonic is the sixth harmonic. There are two sup-harmonics, but they are of small amplitude. In this case, the THD of MMF is 0.325, a small value. Therefore, this new winding can be used for both high-speed and low-speed applications. Under the third harmonic current injection, the working harmonic is the 18th, and its amplitude is smaller than the 10th harmonic, as shown in Figure 4d. In this case, the injection of the third harmonic current will be interesting to improve the output torque for low-speed application.

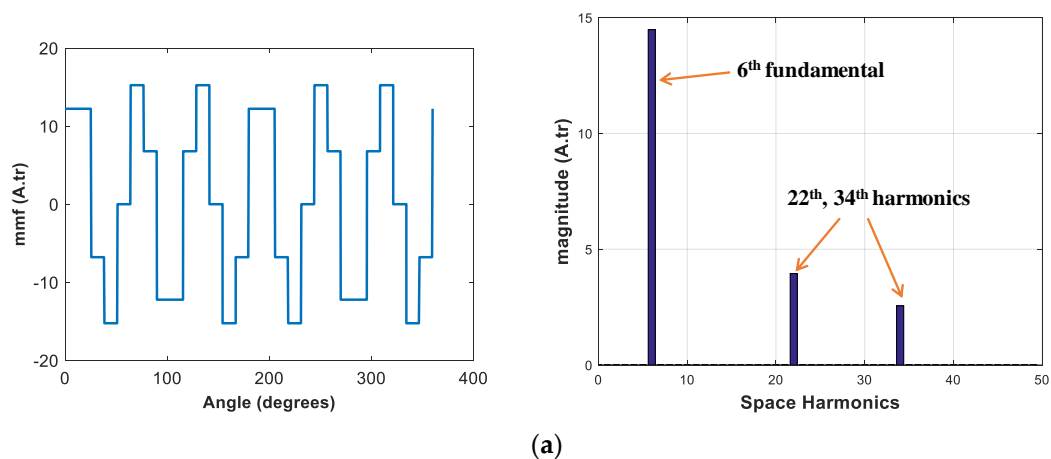


**Figure 4.** Cont.



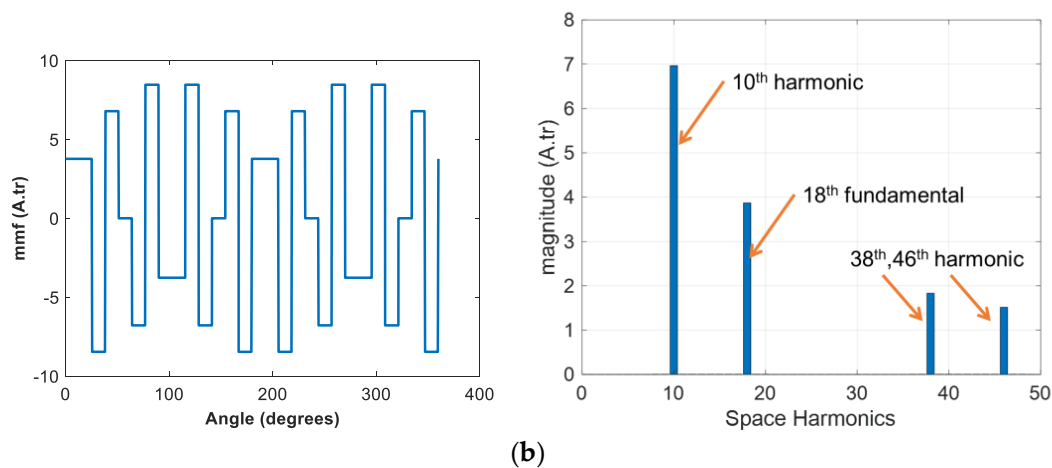


**Figure 4.** MMF harmonic spectrum of seven-phase AFM with fundamental current and third harmonic current: (a) fundamental harmonic; (b) third harmonic.

#### 2.4. Seven-Phase HFM

Based on the seven-phase AFM, a radial rotor with V-shaped PMs embedded is added, as shown in Figure 1d. The same external radius of the rotor is kept compared to the five-phase and three-phase machines. The original idea is to make use of the end windings, and the output torque can be improved. Moreover, in order to extend the operational range, especially for the flux-weakening region, the number of poles of the third rotor is three times than the two axial rotors, i.e., 36 poles. This kind of machine is called a bi-harmonic machine, i.e., the machine can develop output torque of comparable values under three kinds of supply: only fundamental, or only third harmonic, or both the fundamental and the third harmonic current [32]. The synchronous speed of a machine can be obtained using (4). Under the supply of the fundamental current with frequency  $f$ , the number of pole-pairs of the machine is  $p$ , and the synchronous speed is  $n_s$ . When the supply of current is changed to the third harmonic current, i.e., the frequency of current is  $3f$ , the number of pole-pairs to generate output torque is also changed to  $3p$ ; therefore, the synchronous speed is the same as the one with a fundamental current supply. The output torque of the machine is the sum with the supply of the two harmonics of current. This is the reason that the injection of the third harmonic current with multiphase machines can improve the output torque.

$$n_s = \frac{60 \cdot f}{p} \quad (4)$$

In the case of sinusoidal multiphase machines, it is useless to inject third harmonic current, because there is no third harmonic induction of PM. In the case of seven-phase HFM, the third harmonic induction component is reinforced by the third rotor of radial flux, and the injection of the third harmonic of current is useful to improve the output torque. An extra degree of freedom for the control is thus achieved. Under the constraint of the converter, i.e., maximum value of current and voltage, the performance of the machine can be improved, for example, a higher value of torque at low speed and a larger value of maximum speed at the flux-weakening region can be obtained.

### 3. Performance Comparison in Healthy Mode

The four machines in the above section are compared in a quantitative way in this part. The main characteristics in healthy mode are presented, such as the air gap flux density, no-load back emf, field-weakening capability, torque density in terms of mass and volume, and the overload capability.

The objective of this paper is to show the performance comparisons of the four machines with the same outer dimension. The completed machine dimensions are taken into account, i.e., the two end covers of the two radial flux machines and the mechanical part

of the radial part of the axial flux machine are also considered. Table 1 gives the main geometric parameters of the four machines. All four machines have the same stator radius, axial length and air gap length. All the radial flux machines, including the seven-phase HFM, have the same external rotor radius. It should be noted that the four machines do not have the same volume of PMs.

**Table 1.** Main parameters of the four machines.

Items	5-Phase SPM	3-Phase IPM	7-Phase AFM	7-Phase HFM
Stator slots	25	36	28	28
Pole-pairs	11	16	6	6/18
Pole arc coefficient	0.90	0.74	0.89	0.89/0.58
External rotor radius (mm)	100	100	78.7	100
External Stator radius	88.5	88.5	88.5	88.5
Internal Stator radius (mm)	60	60	38.1	38.1
Air gap (mm)	2	2	2	2
Active Axial length (mm)	30	30	53	53
Total axial length (mm)	53	53	53	53
No. of turns of winding by phase	18	10	19	13
PM volume (mm <sup>3</sup> )	46,724.13696	55,449.6	69,574.51358	140,044.5136

Concerning the axial length, the active length of the radial flux machines equals 30 mm. However, the one with the axial and hybrid seven-phase machine is higher (53 mm). Two passive parts (end covers) must be added in order to make a real machine. The dimensions of the two end covers of one five-phase SPM machine are taken as a reference here [26].

### 3.1. No-Load Performance

The used finite element software is Maxwell, and some settings are as follows: the machines are meshed according to the material and location; the max length of the mesh is 1/8 to 1/10 of the default values. For calculation efficiency, the number of elements is limited in 3D FEM. The magnetostatic solver is used for flux density computation and for other parameters, and the transient solver is used.

- Flux density mapping

Figure 5 compares the flux distribution under no-load conditions of the proposed four machines, which is important for the magnetic-circuit design of electrical machines. The same air gap length is employed for the four machines, as shown in Table 1. In the three-phase IPM, there is more flux leakage due to the magnetic bridge. Under the mechanical constraint, the thickness of the magnetic bridge should be designed as thin as possible in order to reduce the flux leakage. In seven-phase machines, the width of back-iron of the rotors is adjusted in order to obtain the same amplitude of flux density as the five-phase SPM.

- Air gap flux density

The amplitudes of the air gap flux density are the same, i.e., 0.8 T, as shown in Figure 6. Figure 6d shows the values in the radial air gap of the seven-phase HFM, and the ones in the two axial air gap are the same as the seven-phase AFM, which are shown in Figure 6c. The results can also be proven by the flux distribution in Figure 5. In electrical machines with low speed applications, a higher value of air gap flux density is often preferred, which leads to a higher value of torque density. The permitted loading level for a machine is often defined on the basis of the saturation value of laminations of both the stator and rotor, the insulation material and the cooling system [33]. The empirical values are employed in order to determine the initial dimensions of the machine, and then, they are adjusted within an iterative process.

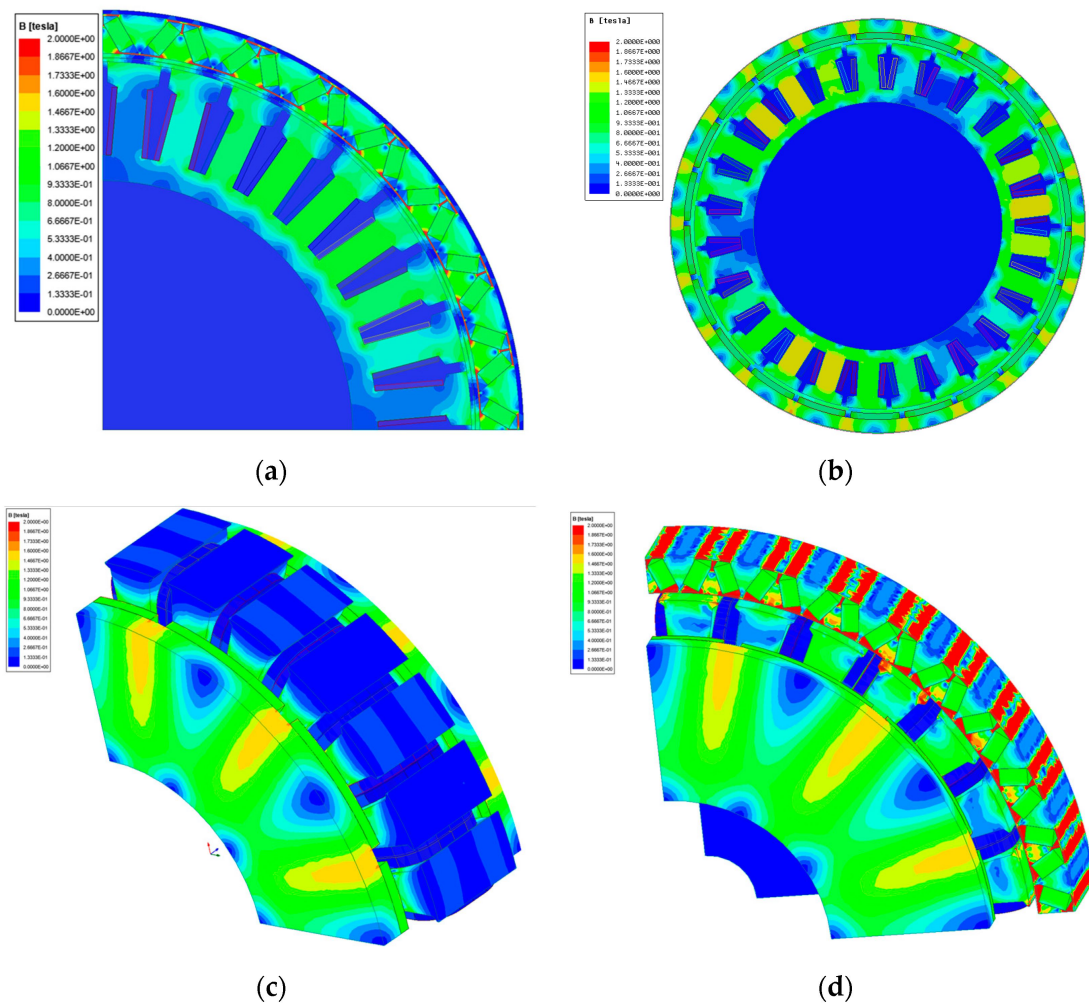


Figure 5. No-load flux density distribution with the same scale bars of (a) three-phase IPM; (b) five-phase SPM; (c) seven-phase AFM; (d) seven-phase HFM.

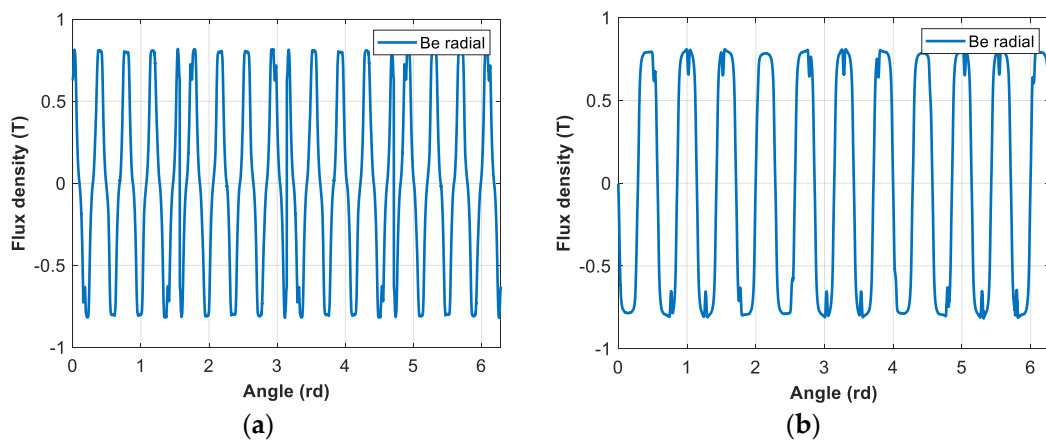
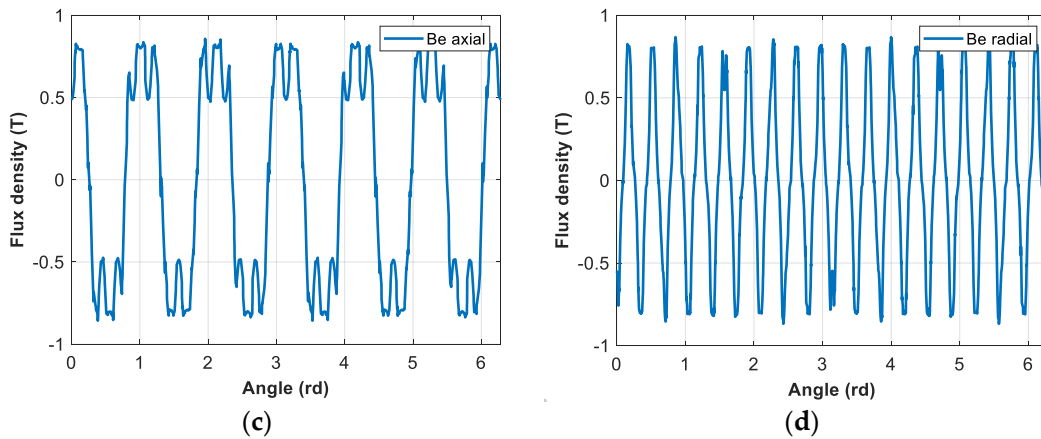


Figure 6. Cont.



**Figure 6.** No-load air gap flux density of (a) three-phase; (b) five-phase; (c) seven-phase AFM; (d) seven-phase HFM radial air gap.

- No-load back-emf

Based on the no-load air gap flux density generated by PMs, the flux linkage can be expressed in (5). Machine winding can perform as a filter through winding factors, i.e., some harmonics of flux density can be reduced or eliminated by adjusting the winding factors.

$$\varphi_h = (\xi_w)_h \cdot l \cdot N_{ph} \cdot \int_0^{\pi/p \cdot h} (B_{rotor})_h \cdot \sin(h \cdot p \cdot \theta) \cdot R_{rotor} \cdot d\theta \quad (5)$$

where  $(\xi_w)_h$  is the winding factor of the  $h$ th harmonic;  $l$  is the active length of the machine;  $N_{ph}$  is the number of turns in series for each phase;  $R_{rotor}$  is the rotor radius.

No-load emf is generated due to the reaction of the variation of flux linkage of PMs, and it can be obtained using (6). Figure 7 shows the no-load emf of the proposed four machines with the speed 600 rpm. The number of turns in series of each machine is adjusted in order to obtain the same amplitude. With the increase in the number of phases, the proportion of the third harmonic of emf increases. Based on the no-load emf, electrical machines can be classified by sinusoidal or non-sinusoidal machines. Three-phase machines are often sinusoidal ones. The third harmonic can also be considered in order to improve the output torque by shaping the PMs [16]. In the case of multi-phase machines, the improvement of performance can be achieved by higher-order harmonics of emf and current.

$$e_i = \frac{d\varphi_i}{dt} \text{ with } i = 1, 2, 3, \dots, m \quad (6)$$

where  $m$  is the number of phases.

- Cogging torque

When the PM machine windings are not fed, the PM generates a magnetic field, and the interaction of the stator teeth produces a force that tries to fix the rotor at a certain position, which will generate an electromagnetic torque, i.e., a cogging torque. The cogging torque changes periodically as the rotor spatial position changes. Cogging torque fluctuation is an inherent phenomenon of the PM machine, which affects the low-speed performance of the machine. Minimization of the cogging torque is one of the goals pursued in the design of high-performance PM machines.

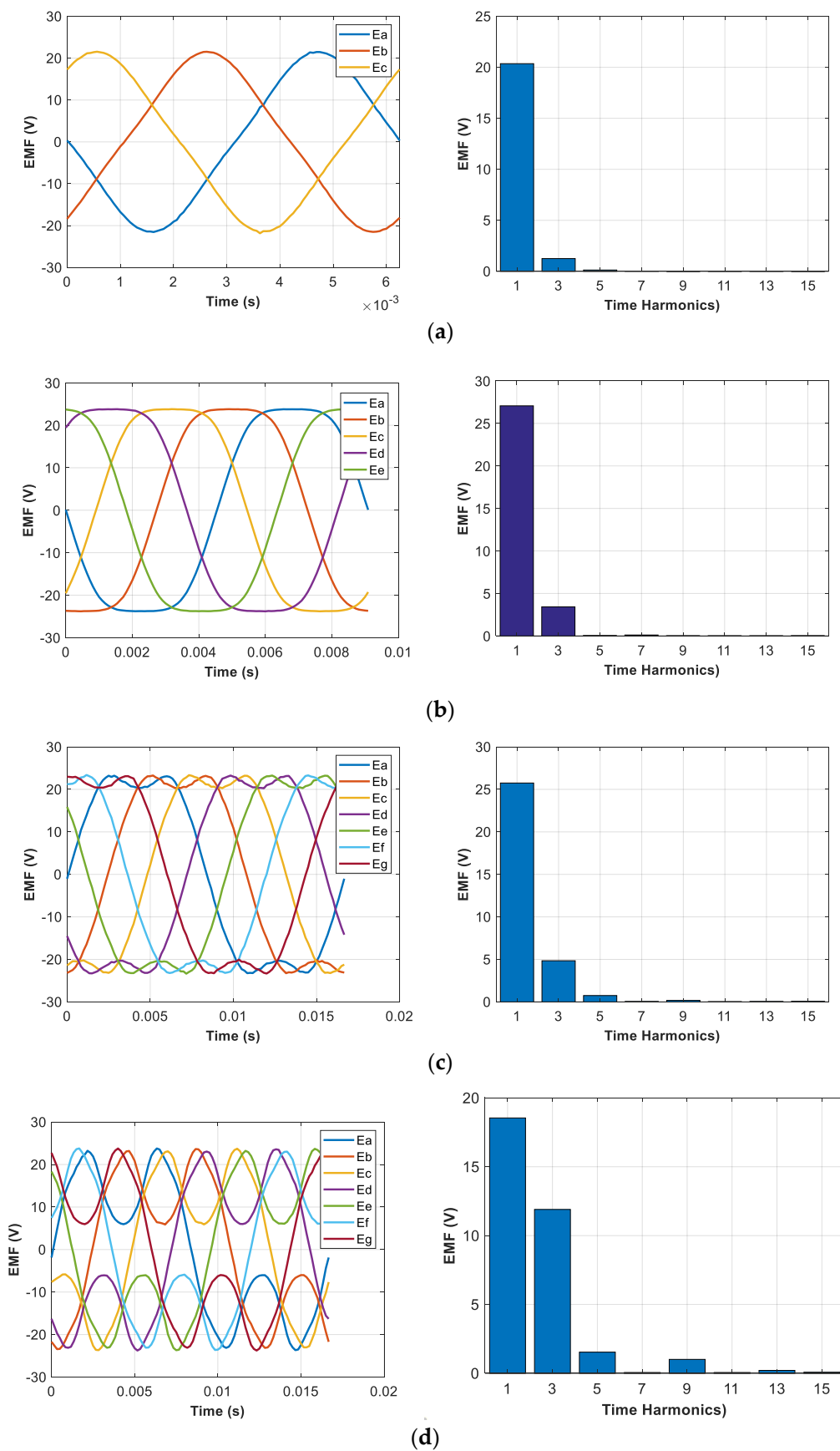


**Figure 7.** EMFs and spectrum harmonics of (a) three-phase IPM; (b) five-phase SPM; (c) seven-phase AFM; (d) seven-phase HFM.

In FSCW machines, the slot/pole number combination plays a major role in determining the cogging torque magnitude [34]. The frequency of cogging torque over the entire machine rotation can be calculated by Equation (7) [35]:

$$f_{\text{cog}} = \text{LCM}(Q, 2p) \quad (7)$$

where  $Q$  is the number of stator slots, and  $\text{LCM}(Q, 2p)$  is the least common multiple of the number of slots  $Q$  and the number of poles  $2p$ . As the frequency of the cogging torque increases, the effect of the torque ripple on the machine output will be reduced, as the magnetic power changes more smoothly around the air gap. Therefore, proper selection of the number of slots and poles can reduce the output torque ripple. Table 2 gives the LCM of the four machines, and Figure 8 shows the cogging torque of the four machines. By comparison, it was found that the cogging torque amplitude of the seven-phase machines are higher than the others, because of the lowest LCM.

**Table 2.** LCM of the four machines.

Items	5-Phase SPM	3-Phase IPM	7-Phase AFM	7-Phase HFM
$\text{LCM}(Q, 2p)$	550	288	84	84

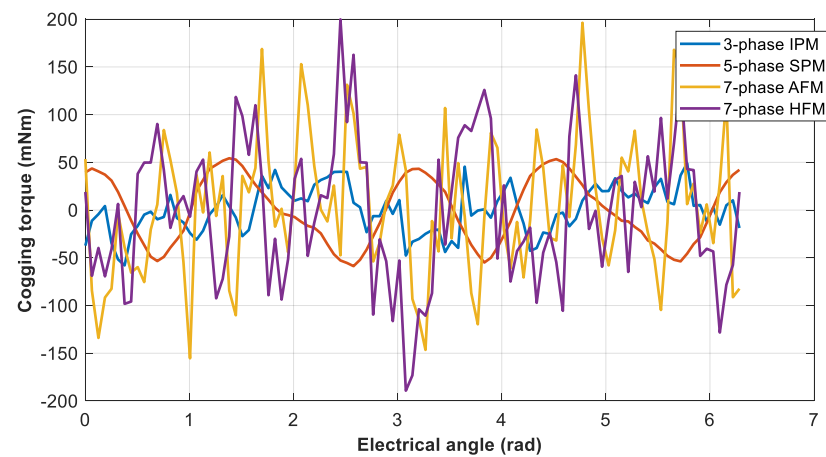


**Figure 8.** The cogging torque of the four machines.

### 3.2. On-Load Performance

Under a constant current supply of  $5 \text{ A/mm}^2$ , Figure 9 compares the steady state torque of the four machines at low speed (120 rpm). As expected, the torque of the seven-phase HFM is the highest. It is 51%, 24% and 13% higher than the three-phase IPM, five-phase SPM and seven-phase AFM, respectively.

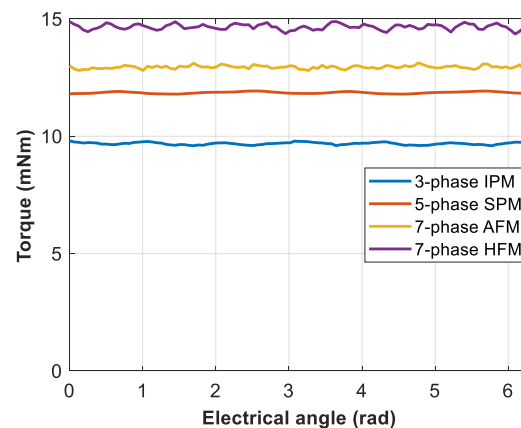


**Figure 9.** Steady state torque analysis: torque at 120 rpm.

The characteristics of the output torques are listed in Table 3. It can be noted that the five-phase SPM machine is the best choice in terms of the torque ripple.

**Table 3.** On-load torque characteristics of the four machines.

Torque (Nm)	5-Phase SPM (Nm)	3-Phase IPM (Nm)	7-Phase AFM (Nm)	7-Phase HFM (Nm)
mean	11.858	9.688	12.938	14.666
Max	11.929	9.8003	13.133	14.889
Min	11.797	9.5956	12.775	14.372
Ripple	1.11%	2.11%	2.77%	3.53%

Where ripple =  $\frac{\max - \min}{\text{mean}}$ .

The overload capability of the machines is related to the acceleration and climbing capabilities of the in-wheel traction applications. Table 4 shows the average output torque of the four machines versus current densities by FEA. It can be noted that the seven-phase HFM output is the highest torque in the whole current density range. It is therefore the seven-phase HFM that exhibits the strongest overload capabilities.

**Table 4.** The average output torque of four machines versus current densities.

Current Density (A/mm <sup>3</sup> )	5-Phase SPM (Nm)	3-Phase IPM (Nm)	7-Phase AFM (Nm)	7-Phase HFM (Nm)
5	11.858	9.688	12.938	14.666
10	23.380	19.272	25.675	29.025
15	33.680	27.934	38.056	42.863
20	42.169	34.397	50.968	57.139

Figure 10 shows the steady state loss analysis. Figure 10a compares the steady state joule losses of the four machines. Compared to the three-phase IPM and the five-phase SPM, the seven-phase machines consider the winding ends; thus, the joule losses in the steady state are larger under a constant current supply of 5 A/mm<sup>2</sup>. Figure 10b compares the steady state core losses of the four machines with the speed 600 rpm. The core loss of the seven-phase AFM is smallest because of its small THD of MMF, which is suitable for high-speed application.

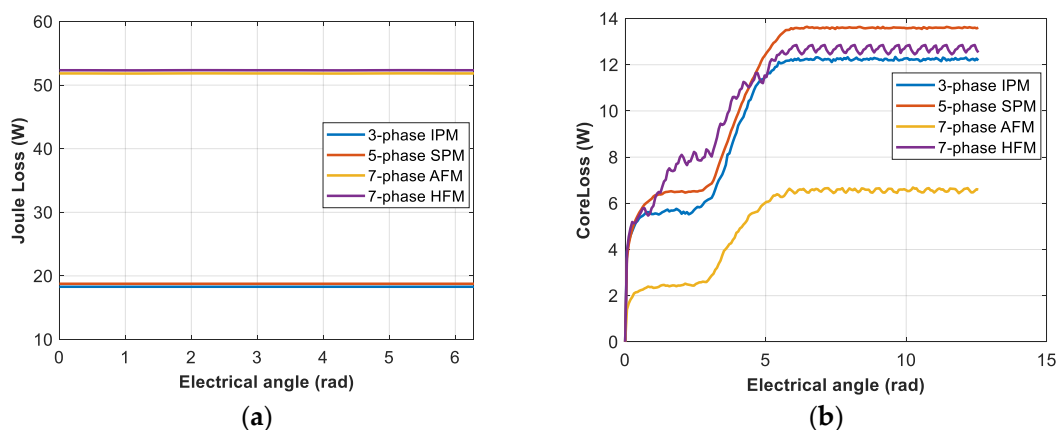


**Figure 10.** Steady state loss analysis: (a) joule losses; (b) core losses.

The steady state on-load losses and the efficiencies are analyzed using FEM, which are listed in Table 5. The mechanical losses are supposed to be 15 W, and it can be noted that all four machines perform well in efficiency, and the seven-phase HFM is the best in terms of efficiency.

**Table 5.** Efficiency of four machines.

	5-Phase SPM (Nm)	3-Phase IPM (Nm)	7-Phase AFM (Nm)	7-Phase HFM (Nm)
Torque (Nm)	11.858	9.688	12.938	14.666
Electric power (W)	745.005	608.670	812.859	921.424
Joule loss (W)	39.403	36.586	51.836	52.336
Core loss (W)	13.6	12.213	6.591	12.798
mechanical loss (W)	15	15	15	15
Efficiency	91.64%	90.51%	91.72%	92.00%

### 3.3. Torque Density

The definition of the torque density can be found in [4]. In order to have a reasonable comparison, the complete machines are considered, e.g., the end windings for the 2D magnetic circuit machines, such as the three-phase IPM and five-phase SPM. Moreover, the axial end closures are also taken into account. Therefore, the four machines have the same volume. It can be seen from Table 6 that the torque density of the seven-phase HFM is the highest not only in mass but also in volume.

**Table 6.** Torque density of the four machines.

Items	5-Phase SPM	3-Phase IPM	7-Phase AFM	7-Phase HFM
Torque (Nm)	11.858	9.688	12.938	14.666
Mass (kg)	7.512	7.377	7.975	8.480
Volume (mm <sup>3</sup> )	1,665,044.106	1,665,044.106	1,665,044.106	1,665,044.106
torque density (Nm/kg)	1.578	1.313	1.622	1.729
torque density (Nm/m <sup>3</sup> )	7121.733	5818.464	7770.365	8808.175

### 3.4. Field Weakening Capability (Inductance/Speed–Torque Curves/Power–Speed Curve/Field Weakening Control Trajectory (MTPA))

Under the assumption of no saturation, no reluctance effect and regular spatial distribution of windings, using a vectorial control approach, a machine of n-phase, wye connected, can be considered to be a set of  $(n - 1)/2$  fictitious two-phase machines [36]. The  $(n - 1)/2$  fictitious machines are magnetically decoupled, and each of them is characterized by a family of harmonics. Table 7 shows the spectrums of harmonics related to the fictitious two-phase machines. Taking the three-phase machine as an example, it is decoupled to a one-phase homopolar machine consisting of  $3k$  harmonics and one two-phase primary machine consisting of  $3k \pm 1$  harmonics,  $k = 0, 1, 2, \dots$ . The two fictitious machines are magnetically decoupled, i.e., the injection of the fundamental current does not interact with the harmonics in the homopolar machine. The interaction between the fundamental current and the fundamental emf framed in Table 5 will generate a constant torque, and the pulsation torque will be generated with other harmonics non-framed. In the case of the five-phase machine, a secondary two-phase fictitious machine can also contribute to the output torque, with the injection of the third harmonic of current.

**Table 7.** Harmonic distribution related to different fictitious machines [36].

No. of Phase	Current Harmonic Injection	EMF Harmonic
3	$h = 1$ (Primary machine)	$\underline{1}, 5, 7, 11, 13, \dots, 3k \pm 1$
	$h = 3$ (Homopolar machine)	$3, 9, 15, 21, 27, \dots, 3k$
5	$h = 1$ (Primary machine)	$\underline{1}, 9, 11, 19, 21, \dots, 5k \pm 1$
	$h = 3$ (Secondary machine)	$\underline{3}, 7, 13, 17, 23, \dots, 5k \pm 3$
	$h = 5$ (Homopolar Machine)	$5, 15, 25, 35, 45, \dots, 5k$
7	$h = 1$ (Primary machine)	$\underline{1}, 13, 15, 27, 29, \dots, 7k \pm 1$
	$h = 3$ (Secondary machine)	$\underline{3}, 11, 17, 25, 31, \dots, 7k \pm 3$
	$h = 5$ (Third machine)	$\underline{5}, 9, 19, 23, 33, \dots, 7k \pm 5$
	$h = 7$ (Homopolar Machine)	$7, 21, 35, 49, \dots, 7k$

□ Framed: generated a constant torque; non-framed: pulsation torque.



The output torque of the  $n$ -phase machine is the sum of torques of fictitious machines, similar to the fictitious machines that are coupled together in a mechanical way. For example, for a five-phase machine, the output torque can be expressed in (8) during the injection of both the fundamental and third harmonic of current. In the case of seven-phase machines, the fifth harmonic can also be used to enforce output torque. However, the fifth harmonic of emf is often tiny, and it is thus not considered.

$$T_e = p(\varphi_{d1}i_{q1} - \varphi_{q1}i_{d1}) + 3p(\varphi_{d3}i_{q3} - \varphi_{q3}i_{d3}) \quad (8)$$

where  $p$  is the number of pole-pairs;  $\varphi_{d1/3}$ ,  $\varphi_{q1/3}$  are the  $d$ - and  $q$ - axis flux;  $i_{d1/3}$ ,  $i_{q1/3}$  are the  $d$ - and  $q$ - axis current, respectively.

The output torque of the four machines are evaluated for the control strategy whose objective is to find the maximum torque under voltage and current limits. An optimization problem is formulated for the control strategy as follows:

$$\begin{aligned} & \max_x (T_e) \\ \text{s.t.} \quad & \max(u_1, u_2, \dots, u_n) \leq U_{DC}/2 \text{ and } n = \{3, 5, \text{ or } 7\} J \leq 5 \text{ A/mm}^2 \\ \text{with} \quad & x = [I_1, \psi_1, I_3, \psi_3] \end{aligned} \quad (9)$$

where  $I_{1/3}$ ,  $\psi_{1/3}$  are the amplitude and phase of the injected currents;  $u_i$ ,  $i = 1, \dots, n$  is the phase voltage;  $U_{DC}$  is the voltage of DC bus;  $J$  is the current density and should be less than  $5 \text{ A/mm}^2$ .

In this case, only one harmonic of current is injected with the three-phase IPM machine and two harmonics of currents, i.e., the first or the third harmonic are injected simultaneously with other multiphase machines. The rms values of current are respected to be the same with all the cases. The torque optimization problem is solved by using the *fmincon* function, a non-linear programming solver to find the minimum (or maximum) of a constrained non-linear multivariable function in MATLAB. The torque-speed characteristics are obtained and shown in Figure 11. It can be shown that the seven-phase HFM machine can develop the highest value of torque. The three-phase IPM machine is characterized by the largest operational speed range. For the three-phase IPM machine, the reluctance torque due to the salient-pole effect helps enlarge the operational speed range.

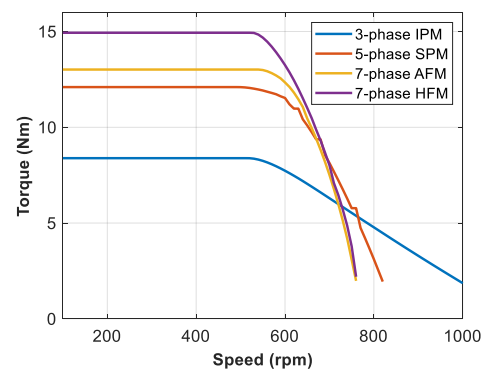


Figure 11. Torque-speed characteristics.

#### 4. Performance Comparison in Degraded Mode

Multiphase machines are intrinsically more reliable than three-phase ones [37]. The fault-tolerant capability of the proposed four machines with one phase open-circuited is investigated. In order to ensure the same rotating magnetic field and a smooth torque, the currents in healthy should be rearranged. Many strategies have been proposed for fault-tolerant control, and the one proposed in [21] is employed here.

For all the machines, it is assumed that the phase A is open-circuited. In order to get a smooth torque, the method for generation of current references in [23,38] is applied in this paper. The new current reference of phase  $m$  in faulty mode  $I_{mf}$  can be expressed as follows:

$$i_{mf} = I_1 \sin(\omega t + \theta_m + \psi_1) + I_3 \sin(3(\omega t + \theta_m + \psi_3)) \tag{10}$$

where  $\theta_m$  is constant initial phase angle of phase  $m$ . For three-phase machine,  $\theta_{b,c} = (\frac{\pi}{2}, -\frac{\pi}{2})$ . For five-phase machine,  $\theta_{b,c,d,e} = (\frac{\pi}{5}, \frac{4\pi}{5}, -\frac{4\pi}{5}, -\frac{\pi}{5})$ . And in case of seven-phase machine,  $\theta_{b,c,d,e,f,g} = (0.3735 \text{ rad}, \frac{\pi}{2}, 2.768 \text{ rad}, -2.768 \text{ rad}, -\frac{\pi}{2}, -0.3735 \text{ rad})$ . Figure 12 shows rearranged current vectors.

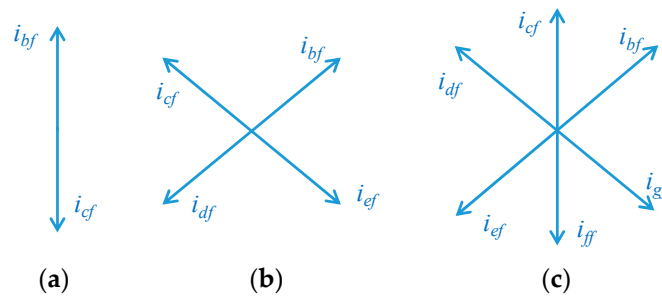


**Figure 12.** New current references with one-phase open-circuited (a) three-phase; (b) five-phase; (c) seven-phase.

The optimization problem in (9) is also used in this part in order to maximize the output torque, but with the phase A current  $i_A = 0$ . The problem will be solved by using the *fmincon* algorithm in cases with the injection of both the fundamental and the third harmonic currents.

Figure 13 shows the machine performances with one phase open-circuited, in which the torque-speed characteristics of the full speed operation is presented in Figure 13a and the torque quality at low speed is shown in Figure 13b. In the case of the one-phase open-circuit, the three-phase machine can still operate without stopping unless the windings are in Delta connection. The magnetic flux in the air gap is elliptical, and the torque ripple is important and will lead to the important vibration of the system. The seven-phase AFM machine can have a better performance in case of the torque ripple and a wide torque-speed operation range. The seven-phase HFM machine exhibits the more interesting performance of the output torque at low speed. Only the case with the one-phase open circuit is investigated. The more phase numbers, the more degree of freedom that can be obtained, i.e., the seven-phase machine is superior to the other machines in the fault tolerant capability.

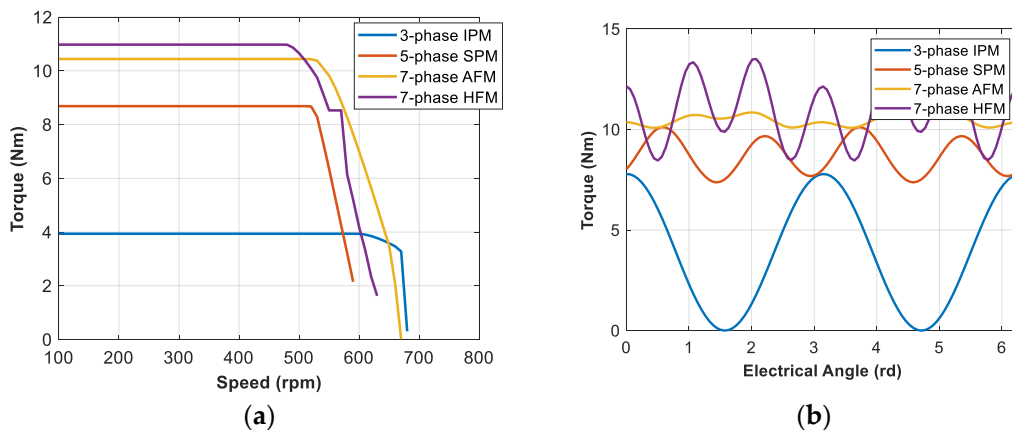


**Figure 13.** Torque characteristics in degraded mode of (a) torque-speed curves; (b) torques at low speed.

## 5. Conclusions

Four electrical machines with different structures and phases were designed and compared for in-wheel electrical vehicle application in this paper. It is clear that the three-phase machine is the least interesting for fault-tolerant operation but also in health operation because of the lower torque density. For a giving quantity of machine volume, the seven-phase HFM machine can exhibit the best torque densities and similar behavior with one open phase. Two types of torque density are also compared in terms of volume and mass, and the seven-phase HFM machine is the best candidate. For the field weakening operation, the IPM machine can achieve the highest speed operation range. Finally, the fault-tolerant capability was investigated. With the higher number of phases, there are more degrees of freedom for the control, and the output torque ripple is less important than the one-phase open circuited one, and it is more interesting for the fault-tolerant operation. Besides the purely technique aspects, generally, the complex structure will make the machine difficult for manufacturing and maintenance. Therefore, the seven-phase HFM machine is the most difficult for manufacturing and maintenance, and the five-phase SPM is much easier for production and maintenance.

**Author Contributions:** J.G., B.Z. and E.S. contributed to the design of the machines, J.G., Y.H. and N.K.N. contributed to the control of the machines. All authors have read and agreed to the published version of the manuscript.

**Funding:** This research was funded by National Natural Science Foundation of China, grant number 52177052, and by the Natural Science Foundation of Shandong Province, grant number ZR2020ME207.

**Data Availability Statement:** MDPI Research Data Policies.

**Conflicts of Interest:** The authors declare no conflict of interest.

## References

1. Husain, I.; Ozpineci, B.; Islam, M.S.; Gurpinar, E.; Su, G.J.; Yu, W.S.; Chowdhury, S.; Xue, L.; Rahman, D.; Sahu, R. Electric Drive Technology Trends, Challenges, and Opportunities for Future Electric Vehicles. *Proc. IEEE* **2021**, *109*, 1039–1059. [[CrossRef](#)]
2. Yao, Y.; Liu, C.; Lee, C.H. Quantitative Comparisons of Six-Phase Outer-Rotor Permanent-Magnet Brushless Machines for Electric Vehicles. *Energies* **2018**, *11*, 2141. [[CrossRef](#)]
3. El-Refaie, A.; Osama, M. High specific power electrical machines: A system perspective. In Proceedings of the 2017 20th International Conference on Electrical Machines and Systems (ICEMS), Sydney, Australia, 8 November 2017; pp. 1–6. [[CrossRef](#)]
4. Galea, M.; Hamiti, T.; Gerada, C. Torque density improvements for high performance machines. In Proceedings of the IEEE Electric Machines & Drives Conference, Chicago, IL, USA, 12–15 May 2013.
5. Wang, J.; Atallah, K.; Zhu, Z.Q.; Howe, D. Modular Three-Phase Permanent-Magnet Brushless Machines for In-Wheel Applications. *IEEE Trans. Veh. Technol.* **2008**, *57*, 2714–2720. [[CrossRef](#)]
6. Xue, X.D.; Cheng, E.K.W.; Ng, T.W.; Cheung, N.C. Multi-Objective Optimization Design of In-Wheel Switched Reluctance Motors in Electric Vehicles. *IEEE Trans. Ind. Electron.* **2010**, *57*, 2980–2987. [[CrossRef](#)]
7. Fan, Y.; Zhang, L.; Huang, J.; Han, X. Design, Analysis, and Sensorless Control of a Self-Decelerating Permanent-Magnet In-Wheel Motor. *IEEE Trans. Ind. Electron.* **2014**, *61*, 4104–4109.
8. Hua, W.; Zhang, H.; Cheng, M.; Meng, J.; Hou, C. An outer-rotor flux-switching permanent-magnet-machine with wedge-shaped magnets for in-wheel light traction. *IEEE Trans. Ind. Electron.* **2017**, *64*, 69–80. [[CrossRef](#)]
9. Yang, Y.; Rahman, M.M.; Lambert, T.; Bilgin, B.; Emadi, A. Development of an External Rotor V-Shape Permanent Magnet Machine for E-Bike Application. *IEEE Trans. Energy Convers.* **2018**, *33*, 1650–1658. [[CrossRef](#)]
10. Zhang, H.; Wei, H.; Wu, Z. Modular Spoke-Type Permanent-Magnet Machine for In-Wheel Traction Applications. *IEEE Trans. Ind. Electron.* **2018**, *65*, 10. [[CrossRef](#)]
11. Cavagnino, A.; Lazzari, M.; Profumo, F.; Tenconi, A. A comparison between the axial flux and the radial flux structures for PM synchronous motors. *IEEE Trans. Ind. Appl.* **2002**, *38*, 1517–1524. [[CrossRef](#)]
12. Yang, Y.P.; Chuang, D.S. Optimal Design and Control of a Wheel Motor for Electric Passenger Cars. *IEEE Trans. Magn.* **2006**, *43*, 51–61. [[CrossRef](#)]
13. Ho, S.L.; Niu, S.; Fu, W.N. Design and Analysis of a Novel Axial-Flux Electric Machine. *IEEE Trans. Magn.* **2011**, *47*, 4368–4371. [[CrossRef](#)]
14. Zhao, Y.; Li, D.; Ren, X.; Qu, R. Investigation of Permanent Magnet Vernier Machines from Armature Field Perspective. *IEEE J. Emerg. Sel. Top. Power Electron.* **2021**, *10*, 2934–2945. [[CrossRef](#)]
15. Liu, G.; Yang, J.; Chen, M.; Chen, Q. Design and experimental validation for direct-drive fault-tolerant permanent-magnet vernier machines. *Sci. World J.* **2014**, *2014*, 241085. [[CrossRef](#)] [[PubMed](#)]

16. Wang, K.; Zhu, Z.Q.; Ombach, G. Torque Enhancement of Surface-Mounted Permanent Magnet Machine Using Third-Order Harmonic. *IEEE Trans. Magn.* **2014**, *50*, 104–113. [[CrossRef](#)]
17. Du, Z.S.; Lipo, T.A. High Torque Density and Low Torque Ripple Shaped-Magnet Machines Using Sinusoidal Plus Third Harmonic Shaped Magnets. *IEEE Trans. Ind. Appl.* **2019**, *55*, 2601–2610. [[CrossRef](#)]
18. Wang, K.; Zhu, Z.Q.; Ombach, G. Torque Improvement of Five-Phase Surface-Mounted Permanent Magnet Machine Using Third-Order Harmonic. *IEEE Trans. Energy Convers.* **2014**, *29*, 735–747. [[CrossRef](#)]
19. Chen, H.; Liu, X.; Demerdash, N.A.O.; El-Refaie, A.M.; Zhao, J.; He, J. Comparison and Design Optimization of a Five-Phase Flux-Switching PM Machine for In-Wheel Traction Applications. *IEEE Trans. Energy Convers.* **2019**, *34*, 1805–1817. [[CrossRef](#)]
20. Barrero, F.; Duran, M.J. Recent Advances in the Design, Modeling, and Control of Multiphase Machines—Part I. *IEEE Trans. Ind. Electron.* **2016**, *63*, 449–458. [[CrossRef](#)]
21. Fu, J.R.; Lipo, T.A. Disturbance Free Operation of a Multiphase Current Regulated Motor Drive with an Opened Phase. *IEEE Trans. Ind. Appl.* **1994**, *30*, 1267–1274.
22. Mohammadpour, A.; Parsa, L. Global Fault-Tolerant Control Technique for Multiphase Permanent-Magnet Machines. *IEEE Trans. Ind. Appl.* **2015**, *51*, 178–186. [[CrossRef](#)]
23. Vu, D.T.; Nguyen, N.K.; Semail, E.; Moraes, T.J.D.S. Control strategies for non-sinusoidal multiphase PMSM drives in faulty modes under constraints on copper losses and peak phase voltage. *IET Electr. Power Appl.* **2019**, *13*, 1743–1752. [[CrossRef](#)]
24. Vu, D.T.; Nguyen, N.K.; Semail, E. An Overview of Methods using Reduced-Ordered Transformation Matrices for Fault-Tolerant Control of 5-phase Machines with an Open Phase. In Proceedings of the IEEE International Conference on Industrial Technology (ICIT), Melbourne, VIC, Australia, 13–15 February 2019; pp. 13–15.
25. Liu, G.; Lin, Z.; Zhao, W.; Chen, Q.; Xu, G. Third Harmonic Current Injection in Fault-Tolerant Five-Phase Permanent-Magnet Motor Drive. *IEEE Trans. Power Electron.* **2018**, *33*, 6970–6979. [[CrossRef](#)]
26. Falco eMotors. Available online: <https://www.electricbicycleworld.com/> (accessed on 13 February 2019).
27. Zhang, H.; Zhao, B.; Gong, J.; Xu, Y.; Vu, D.T.; Nguyen, N.K.; Semail, E.; Moraes, T.J.D.S. Torque Optimization of a Seven-Phase Bi-harmonic PMSM in Healthy and Degraded Mode. In Proceedings of the 2019 22nd International Conference on Electrical Machines and Systems (ICEMS), Harbin, China, 11–14 August 2019; pp. 1–6. [[CrossRef](#)]
28. El-Refaie, A.M. Fractional-Slot Concentrated-Windings Synchronous Permanent Magnet Machines: Opportunities and Challenges. *IEEE Trans. Ind. Electron.* **2010**, *57*, 107–121. [[CrossRef](#)]
29. Wang, J.; Yuan, X.; Atallah, K. Design Optimization of a Surface-Mounted Permanent-Magnet Motor with Concentrated Windings for Electric Vehicle Applications. *IEEE Trans. Veh. Technol.* **2013**, *62*, 1053–1064. [[CrossRef](#)]
30. Scuiller, F.; Semail, E.; Charpentier, J.-F. General modeling of the windings for multi-phase ac machines. *Eur. Phys. J. Appl. Phys.* **2010**, *50*, 135–151. [[CrossRef](#)]
31. Reddy, B.; Huh, K.-K.; El-Refaie, A.M. Generalized Approach of Stator Shifting in Interior Permanent-Magnet Machines Equipped with Fractional-Slot Concentrated Windings. *IEEE Trans. Ind. Electron.* **2014**, *61*, 5035–5046. [[CrossRef](#)]
32. Gong, J.; Zahr, H.; Semail, E.; Trabelsi, M.; Aslan, B.; Scuiller, F. Design Considerations of Five-Phase Machine with Double p/3p Polarity. *IEEE Trans. Energy Convers.* **2019**, *34*, 12–24. [[CrossRef](#)]
33. Pyrhönen, J.; Jokinen, T.; Hrabovcova, V. *Design of Rotating Electrical Machines*; John Wiley & Sons, Ltd.: Hoboken, NJ, USA, 2008; ISBN 978-0-470-69516-6.
34. Aslan, B.; Semail, E.; Korecki, J.; Legranger, J. Slot/pole Combinations Choice for Concentrated Multiphase Machines dedicated to Mild-Hybrid Applications. In Proceedings of the Conference of the IEEE Industrial Electronics Society, Melbourne, VIC, Australia, 7–10 November 2011; IEEE: New York, NY, USA, 2011.
35. Fornasiero, E.; Alberti, L.; Bianchi, N.; Bolognani, S. Considerations on selecting fractional-slot windings. In Proceedings of the 2010 IEEE Energy Conversion Congress and Exposition, Atlanta, GA, USA, 12–16 September 2010; pp. 1376–1383.
36. Semail, E.; Kestelyn, X.; Bouscayrol, A. Right Harmonic Spectrum for the back-electromotive force of a n-phase synchronous motor. In Proceedings of the IEEE Industrial Application Society Annual Meeting, Seattle, WA, USA, 3–7 October 2004; pp. 1–8. [[CrossRef](#)]
37. Levi, E. Advances in Converter Control and Innovative Exploitation of Additional Degrees of Freedom for Multiphase Machines. *IEEE Trans. Ind. Electron.* **2015**, *63*, 433–448.
38. Hussein, Z.; Jinlin, G.; Eric, S.; Franck, S. Comparison of Optimized Control Strategies of a High-Speed Traction Machine with Five Phases and Bi-Harmonic Electromotive Force. *Energies* **2016**, *9*, 952.